DOI: 10.1002/chem.200701152

Selective Inclusion of Cu^+ and Ag^+ Electron-Rich Metallic Cations within Supramolecular Polyoxometalates Based on $\{AsW_9O_{33}\}\{Mo_3S_4\}$ Combinations

Sylvain Duval,[a] Marie-Anne Pilette,[a] Jérôme Marrot,[a] Corine Simonnet-Jégat,[a] Maxim Sokolov,*[b] and Emmanuel Cadot*[a]

Abstract: Coordination of the $[Mo_3S_4(H_2O)_9]^{4+}$ cluster with the trivacant $[AsW_9O_{33}]^{9-}$ ion gives the supramolecular complex $[\{(H_4AsW_9O_{33})_4(Mo_3S_4\{H_2O\}_5)\}_2]^{12-}$ (**1**) in good yield. The structure of **1** shows that two $[H_4AsW_9O_{33}]^{5-}$ subunits sandwich a single central $[Mo_3S_4(H_2O)_5]^{4+}$ ion to give a basic monomeric unit $[(H_4AsW_9O_{33})_2\{Mo_3S_4(H_2O)_5\}]^{6-}$. In the solid sate, a supramolecular dimeric association is evidenced that consists of two $[(H_4AsW_9O_{33})_2\{Mo_3S_4(H_2O)_5\}]^{6-}$ units held together by twelve hydrogen bonds and four S···S contacts. Complex **1** reacts with $NaAsO_2$, $AgNO_3$ and CuI to give compounds **2**, **3** and **4**, respectively. X-ray structural analysis reveals that the molecular arrangements of **2** to **4** are closely related to the parent structure of **1**. $\{AsOH\}^{2+}$, Ag^+ and Cu^+ ions are located on three distinct pairs of sites. Two hanging $\{AsOH\}^{2+}$ groups in **2** are symmetrically attached to two opposite $\{AsW_9O_{33}\}$ subunits. Complex **3** is the first example of an $Ag/\{Mo_3S_4\}$ combination in which the environment of the two equivalent Ag^+ cations is remarkable for containing two sulfur atoms belonging to $\{Mo_3S_4\}$, two oxygen and one central arsenic atom of the $\{AsW_9O_{33}\}$ subunits. Potentiometric titration shows that the addition of Ag^+ ions is quantitative and occurs in two successive steps ($K_1 = 4.1 \times 10^6$ and $K_2 = 2.3 \times 10^5\ L\,mol^{-1}$), which is consistent with the retention of the supramolecular cluster in solution. The structure of **4** reveals a single copper atom embedded in the central part of the dimer. The Cu^+ cation is bound to four sulfur atoms to complete a cuboidal moiety. UV/Vis studies in solution indicate that the stability of the dimeric assemblies of **2**, **3** and **4** is significantly enhanced by the presence of Cu^+ or Ag^+ ions, which act as additional coordination linkers within the supramolecular cluster. The anions **1** to **4** were characterised by ^{183}W NMR spectroscopy in solution. The 10-line spectra recorded for each of them are consistent with an averaged C_{2h} molecular symmetry in solution.

Keywords: chalcogens · cluster compounds · molybdenum · polyoxometalates · tungsten

Introduction

The deliberate synthesis of large clusters from stable building blocks is a promising, but still poorly explored approach to the design of inorganic materials with specific sizes and properties.[1] Polyoxometalate (POM) compounds appear to be good candidates for such synthetic concepts. This class of material has stimulated much research activity in a range of scientific fields, such as catalysis, medicine or materials science.[2] Polyoxometalates offer the possibility of combining stereospecific elements, mainly transition-metal cations, in structurally diverse multi-unit assemblies. Such enormous potential has given rise to numerous compounds with specific properties, for example, magnetism, redox activity, optical properties and acidity, for applications in many areas. The richness and diversity of the lacunary (or defect) polytungstates have attracted attention for their use as rigid ligands.[3] A simple (but highly creative) approach to their synthesis is based upon the reactions of defect polyanions with mononuclear aqua cations.[4] Similar coordination processes can be achieved with stable polynuclear aqua cations.[5] In such a context, chalcogen-bridged cluster–aqua complexes such as

[a] S. Duval, Dr. M.-A. Pilette, Dr. J. Marrot, Dr. C. Simonnet-Jégat, Prof. E. Cadot
Université de Versailles Saint Quentin
Institut Lavoisier de Versailles, ILV, UMR CNRS 8180
45 Avenue des Etats-Unis, 78035 Versailles Cedex (France)
Fax: (+33) 139-254-381
E-mail: cadot@chimie.uvsq.fr

[b] Dr. M. Sokolov
Nilolayev Institute of Inorganic Chemistry
Siberian Branch of the Russian Academy of Sciences
Prospect Lavrentieva 3, Novosibirsk 630090, Russia
Fax. (+7) 383-330-9489
E-mail: caesar@che.nsk.su

Supporting information for this article is available on the WWW under http://www.chemeurj.org/ or from the author.

$[Mo_2O_2S_2(H_2O)_6]^{2+}$,[6] $[Mo_3S_4(H_2O)_9]^{4+}$[7] or $[Mo_4S_4(H_2O)_{12}]^{n+}$ $(n=4–6)$[8] form stable polymetallic cations.[9] The combination of chalcogenides and polyoxometalates has already proven to be efficient in the design of sulfur-containing polyoxothiometalate derivatives.[10] Thus, reactions between $[Mo_3S_4(H_2O)_9]^{4+}$ and the monovacant $[SiW_{11}O_{39}]^{8-}$ or $[P_2W_{17}O_{61}]^{10-}$ or the divacant γ-$[SiW_{10}O_{36}]^{8-}$ ion have been reported.[11,12] Trinuclear $\{Mo_3S_4\}$-based clusters are able to incorporate about 22 various transition and post-transition metals (M′) to give a series of mixed-metal cuboidal $\{Mo_3M'S_4\}$ cores.[13] In particular, the stable $[Mo_3(CuCl)S_4(H_2O)_9]^{4+}$ ion is easily obtained from $[Mo_3S_4(H_2O)_9]^{4+}$ and polymeric CuCl.[14] The palladium-containing cuboidal clusters $\{Mo_3PdS_4\}^{4+}$ exhibit unique electronic properties and reactivity that are comparable to Pd(0)-based complexes.[15] They are efficient in alkyne nucleophilic addition reactions and in the isomerisation of hydrophosphoryl molecules into unstable hydroxyphosphine tautomers.[16] Thereby, such $\{Mo_3S_4\}$-containing polyoxometalates could develop cooperative properties that arise from the individual components. The reduced chalcogenide cores are expected to coordinate electron-rich centres, whereas polyoxometalate subunits are known for their electron-storage capacity.

Herein we report the formation and characterisation of supramolecular POM complexes bridged by a $\{Mo_3S_4\}$ core. Direct coordination of $[Mo_3S_4]^{4+}$ to $[AsW_9O_{33}]^{9-}$ leads to a 1:2 covalent monomer that dimerises to give a supramolecular assembly, $[(H_4AsW_9O_{33})_4\{Mo_3S_4(H_2O)_5\}_2]^{12-}$ (**1**), through directed hydrogen bonds and S···S van der Waals interactions.[17] Such a supramolecular arrangement contains three different sets of coordination sites that are able to bind specifically the $\{AsOH\}^{2+}$, Ag^+ and Cu^+ cations. The X-ray structures show that the dimeric arrangement is maintained within the three resulting complexes, $[\{(H_2As_2W_9O_{34})(H_4AsW_9O_{33})(Mo_3S_4\{H_2O\}_5)\}_2]^{14-}$ (**2**), $[\{Ag_2(H_2As_2W_9O_{34})(H_2AsW_9O_{33})(Mo_3S_4\{H_2O\}_5)\}_2]^{16-}$ (**3**) and $[Cu\{(H_2As_2W_9O_{34})(H_4AsW_9O_{33})(Mo_3S_4\{H_2O\}_5)\}_2]^{13-}$ (**4**). Complex **3** represents the first example of an $Ag^+/\{Mo_3S_4\}$ combination. Potentiometry shows that the coordination of Ag^+ proceeds in two successive steps, consistent with the retention of the supramolecular architecture in solution. Furthermore, UV/Vis studies of the anions **2** to **4** reveal that supramolecular dimers are significantly stabilised in the presence of the Ag^+ and Cu^+ cations which act as additional linkers between the two monomeric subunits.

Results and Discussion

Structures of the anions

*$K_3(NH_4)_9[\{(H_4AsW_9O_{33})_2(Mo_3S_4\{H_2O\}_5)\}_2]\cdot 48H_2O$ (**KNH_4-1**)*: The molecular structure of **1** is described as a sandwich-type compound with two $\{AsW_9O_{33}\}$ subunits bound to one $\{Mo_3S_4\}$ cation (Figure 1a). The non-equivalent $\{AsW_9O_{33}\}$ moieties act as bidentate ligands. One is chelating, that is, two terminal oxygen atoms coordinate a single molybdenum atom with the expected Mo–O bond lengths (2.114(8)–2.115(7) Å), whereas the other bridges the two remaining molybdenum atoms (Mo–O = 2.078(8)–2.087(8) Å). The coordinating oxygen atoms of the two $\{AsW_9O_{33}\}$ subunits occupy four equatorial positions within the $\{Mo_3S_4\}$ core. Water molecules are attached to the five remaining coordination sites through longer Mo–O bonds (2.167(8)–2.224(8) Å). Each $\{AsW_9O_{33}\}$ subunit contains four terminal oxygen atoms with W–O bonds long enough for these terminal oxygen atoms to be considered protonated (W–OH = 1.819(10)–1.898(9) Å). The presence of four terminal hydroxo groups per $\{AsW_90_{33}\}$ subunit is consistent with the elemental analysis (six countercations per monomer) and with the averaged bond valence sum (BVS) values of 1.18 ± 0.07 calculated for the oxygen atoms involved. The anion arrangement appears to be stabilised by four intramolecular hydrogen bonds that involve the aquo ligands of the molybdenum atoms and the terminal hydroxo groups adjacent to the coordinated oxygen atoms. The short O···O distances that range from 2.58(1) to 2.72(1) Å reflect the strength of these intramolecular hydrogen bonds.

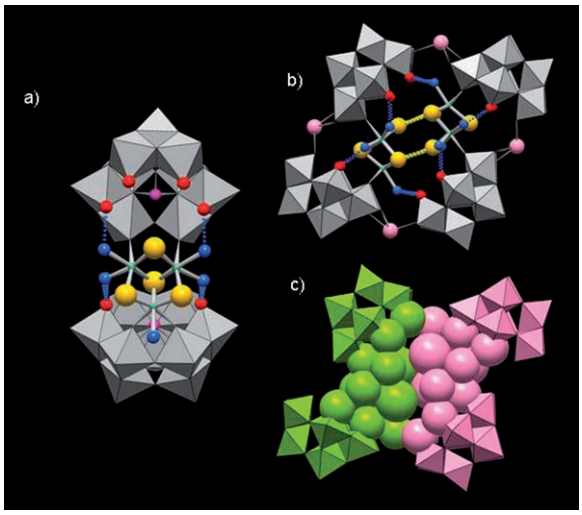

Figure 1. Structure of **1**. a) and b) Mixed polyhedral ($\{AsW_9O_{33}\}$ subunits) and ball-and-stick representations ($\{Mo_3S_4\}$ cores). Mo: green spheres, S: yellow spheres, O: red spheres, As: fuchsia spheres, K: pink spheres and diprotonated oxygen atoms (aquo ligands): blue spheres. a) Face view of the monomer showing the sandwich arrangement. b) Side view of the dimer showing the intermolecular interactions (dotted lines) between the monomeric subunits. c) Representation highlighting the close-packing arrangement (space-filling model) between the two monomers coloured in green and pink for clarity.

The next level in the molecular organisation of **1** corresponds to a supramolecular assembly between two basic monomeric units, which gives rise to a striking head-to-tail arrangement (Figure 1b and c). In the resulting dimeric association, both monomers are equivalent and are related by an inversion centre. They interact mutually through four short intermolecular hydrogen bonds ((O···O) = 2.65(2)–2.71(2) Å) between the remaining attached water molecules and terminal hydroxo groups of the POM subunits. Further-

more, four short van der Waals S···S contacts (3.414(4)–3.488(4) Å) reinforce the intermolecular interactions. Finally, four peripheral potassium ions bridge the four $\{AsW_9O_{33}\}$ subunits through K–O bonds (2.79(1)–3.36(2) Å). The supramolecular structure of **1**, built upon intra- and intermolecular weak interactions, that is, 12 hydrogen bonds that involve all five of the attached aquo ligands, four S···S van der Waals contacts that involve the three μ_2-S atoms of each central $\{Mo_3S_4\}$ core and ionic interactions through K–O bonds, makes compound **1** remarkable in the field of the polyoxometalate chemistry.

*$K_8(NH_4)_6[\{(H_2As_2W_9O_{34})_2(H_4AsW_9O_{33})_2(Mo_3S_4[H_2O]_5)\}_2]\cdot 48H_2O$ (**KNH_4-2**)*: The structure of **2** derives from the parent anion **1** (Figure 2). Nevertheless, two peripheral

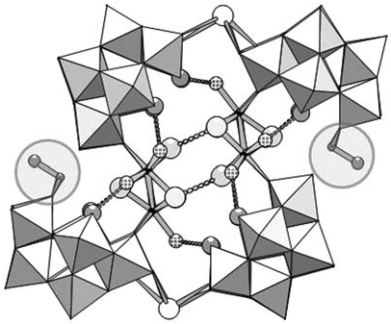

Figure 2. Structure of **2** showing the two equivalent hanging groups attached to two opposite $\{AsW_9O_{33}\}$ subunits. Mo: small black spheres, S: large light grey spheres, O: medium grey spheres, As: small grey spheres, K: large white spheres and diprotonated oxygen atoms (aquo ligands): hatched medium grey spheres.

hanging $\{AsOH\}^{2+}$ groups are grafted onto two opposite $\{AsW_9O_{33}\}$ subunits through a formal substitution of two protons in **1** for one $\{AsOH\}^{2+}$ group. Of the two W–O terminal bonds in the vicinity of the $\{AsOH\}^{2+}$ groups, one is long enough (1.957(4) Å) to be considered as protonated, whereas the other exhibits bond lengths (1.741(5) Å) consistent with a double bond W=O character. Thereby, these structural observations, supported by elemental analysis, lead to an overall charge of −14 per dimer. The coordination sphere of the outer As^{III} atom is completed by a terminal hydroxo group ((As–OH) = 1.780(5) Å) to give the expected trigonal arrangement usually observed in arsenites. For instance, the anion β-$\{HAs_2W_8O_{31}\}^{7-}$ contains such a peripheral $\{AsO_3\}$ trigonal group with similar geometry.[18] All of the intermolecular interactions depicted in **1** are maintained in **2** (Figure 2).

*$K_{16}[\{Ag(H_2As_2W_9O_{33})(H_2AsW_9O_{33})(Mo_3S_4[H_2O]_5)\}_2]\cdot 48H_2O$ (**K-3**)*: The overall supramolecular architecture described above for **1** and **2** is maintained in **3** (Figure 3a). However, two equivalents of coordinated Ag^+ ions are observed, in agreement with the 2:1 stoichiometry evidenced by potentiometric and UV/Vis titrations (see below). The Ag^+ ion

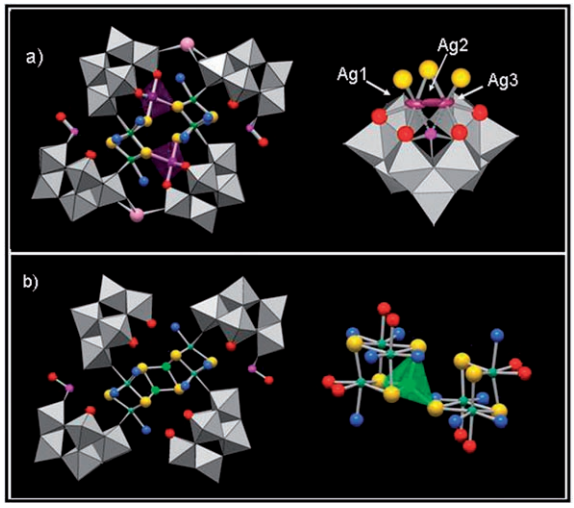

Figure 3. a) Structure of anion **3**. Left: the two coordinated Ag^+ ions (violet spheres and polyhedra) are located in a mixed site composed of two oxygen atoms (red spheres) and the lone pair of the As^{III} atom (fuchsia spheres) belonging to the $\{AsW_9O_{33}\}$ moiety and two sulfur atoms (yellow spheres) of the $\{Mo_3S_4\}$ cores. Right: the silver ions are disordered over three nearby positions labelled Ag1, Ag2 and Ag3 with an occupancy factor of 0.42, 0.15 and 0.42, respectively. b) Structure of anion **4**. Left: the single Cu^+ ion (green spheres) is equally disordered over two equivalent positions within a central pocket. Right: magnified view of the central arrangement of anion **4** highlighting the distorted tetrahedral arrangement of the Cu^+ ion.

appears to be disordered over three nearby positions labelled Ag1, Ag2 and Ag3 (see Figure 3a). The two main sites, Ag1 and Ag3 (statistical occupancy factor, SOF = 0.42), appear to be quite equivalent (strictly equivalent in the idealised C_{2h} symmetry). Between the Ag1 and Ag3 atoms, a weak electronic density was found and refined as a silver atom (Ag2) with an occupancy factor of 15%. The thermal vibration ellipsoids of the three silver positions are oblate along a common direction, which suggests a dynamic disorder (hopping) of the Ag^+ ion between the two main sites Ag1 and Ag3, crossing over the central Ag2 position. Such fluxional behaviour, suspected in the solid state, is evidenced in solution by ^{183}W NMR spectroscopy (see the ^{183}W NMR Spectroscopy section below). The coordination sphere of the Ag^+ cation, when located on the two main sites Ag1 and Ag3, contains two oxygen atoms and two sulfur atoms (Figure 3a). The shortest Ag–O (2.220(13)–2.260(13) Å) and Ag–S (2.463(5)–2.485(5) Å) bonds are arranged in a quasi-linear bridge (≈177°), whereas the other two longer Ag–O and Ag–S bonds (2.459(13)–2.521(14) and 2.635(5)–2.652(6) Å, respectively) are arranged in a closer O–Ag–S junction (≈104°). In addition, the short Ag–As distances (2.727(4)–2.770(5) Å) suggest a bonding interaction with the lone-pair of the central As^{III} atom of the $\{AsW_9O_{33}\}$ subunit. The presence of the two encapsulated Ag^+ ions is expected to reinforce significantly the intermolecular association because, in addition to the weak hydrogen bonds and S···S interactions, the silver ions appear to act as two additional linkers between the two monomers (Figure 3). Of the oxygen and sulfur atoms coordinating the Ag^+ ion, three

(2O+S) belong to the same monomer and the complementary monomer supplies the remaining sulfur atom. Herein, the supramolecular architecture is required to create coordination sites for the Ag^+ ions. The elemental analysis of **K-3** reveals eight K^+ ions per monomer, which is consistent with the presence of three protons. One proton is unambiguously located on one of the W–O bonds neighbouring the {AsOH} group (W–O = 1.942(11 Å) while the two remaining protons are probably distributed over the four terminal oxygen atoms in the vicinity to the disordered Ag^+ ion (W–O = 1.822(11)–1.845(11) Å).

*$K_{13}[Cu\{(H_2As_2W_9O_{33})(H_4AsW_9O_{33})(Mo_3S_4[H_2O]_5)\}_2]\cdot 43\,H_2O$ (**K-4**)*: Anion **4** (Figure 3b) exhibits the characteristic intermolecular arrangement already observed for **1** to **3**. According to the synthetic procedure, a single Cu^I atom appears equally distributed over two equivalent sites separated by a short distance (2.335(6) Å). The Cu^+ ion interacts with four sulfur atoms and displays a distorted tetrahedral geometry if the Mo–Cu interactions (2.759(3)–2.876(3) Å) are ignored (Figure 3b). The four Cu–S bonds exhibit the expected lengths (2.137(4)–2.285(4) Å). In addition to the intermolecular interactions, one Cu–S bond participates in the supramolecular cohesion. Double heterometallic cuboidal arrangements have been found with two Cu^I, for example, $[\{Mo_3CuS_4(H_2O)_9\}_2]^{8+}$, but this is a reduced paramagnetic cluster with formal oxidation states IV, IV and III for the Mo_3 units.[19] In this case, the two copper ions interact through short Cu–Cu bonds (2.43 Å), but this is 0.1 Å longer than the Cu–Cu separation observed in anion **4**.

Synthesis of anions 1 and 2: The monomer $[(H_4AsW_9O_{33})_2\text{-}\{Mo_3S_4(H_2O)_5\}]^{6-}$ is formed in a straightforward way by ligand-exchange reactions in the presence of stoichiometric amounts of $[Mo_3S_4(H_2O)_9]^{4+}$ and $[AsW_9O_{33}]^{9-}$. The pH must be maintained in the range of 2–3 because the chalcogenide cluster tends to form (irreversibly) insoluble condensation products at a higher pH, whereas $[AsW_9O_{33}]^{9-}$ degrades quickly in a more acidic medium (pH < 2). Under such conditions, the four remaining terminal oxygen atoms of the $\{AsW_9O_{33}\}$ subunits are protonated which prevents any further condensation. Anion **1** reacts with two equivalents of sodium arsenite to give anion **2** at pH 2.

Solution studies

*UV/Vis spectrum, stability and complexation properties of **2***: The behaviour of **2** in solution was studied by UV/Vis spectroscopy. The absorptions between 800 and 350 nm are attributed to the $\{Mo_3S_4\}$ chromophore (charge-transfer transition between sulfur and molybdenum and d–d transitions) because the $\{AsW_9O_{34}\}$ moiety absorbs only in the UV domain below 300 nm (Figure 4). The molar absorption ε of **2** measured at the 620 nm maximum (calculated for 1 mol L^{-1} in $\{Mo_3S_4\}$) increases significantly from about 550 to 1100 L mol^{-1} cm^{-1} as the concentration increases from 5×10^{-4} to 5×10^{-3} mol L^{-1} (Figure 5). Such a feature is related

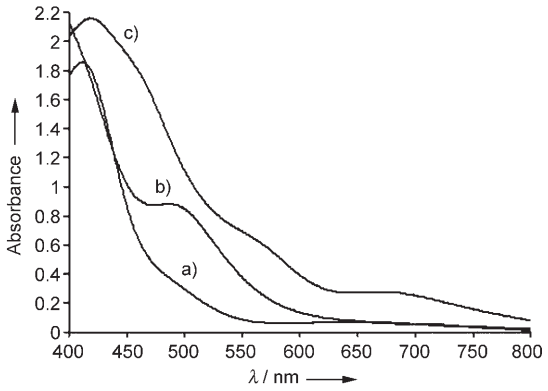

Figure 4. Electronic absorption spectra of a) **2** (3.2 mM), b) **2** (3.2 mM) + CuI (2 equiv) and c) **2** (3.2 mM) + $AgNO_3$ (2 equiv).

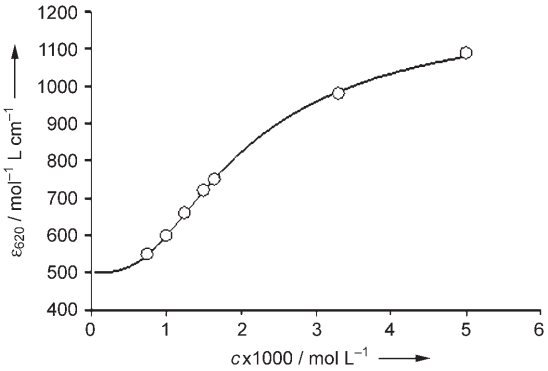

Figure 5. Variation of the molar absorption of **2** at 620 nm upon concentration. Experimental (○) and values calculated for $K_d(3) = 930$ (——) are shown.

to changes in the environment of the $\{Mo_3S_4\}$ core, which is consistent with the presence of an equilibrium between the monomeric moiety (denoted M^{7-}) and the dimer **2** (denoted M_2^{14-}) [Eq. (1)].

$$M_2^{14-} \rightleftharpoons 2M^{7-} \quad (1)$$

As already shown for other $\{Mo_3S_4\}$-based systems, the electronic properties of the incomplete cuboidal $\{Mo_3S_4\}^{4+}$ are strongly dependent upon the nature of the ligands that surround the three molybdenum atoms. For instance, the first ionisation of $[Mo_3S_4(H_2O)_9]^{4+}$ ($K \approx 0.018$) leads to a slight decrease in absorbance below pH 1, whereas at higher pH the large absorption increases are attributed to further deprotonation and oligomerisation processes.[20] Therefore, the significant absorption changes observed in the visible region should be as a result of changes in the outer-sphere of the molybdenum atoms in **2** that arise from the breaking or formation of weak interactions (hydrogen bonds and van der Waals S···S contacts). The UV/Vis data (ε_{620} vs. concentration in **2**) allow the fraction of dimer (α) to be determined by Equation (2) (for details, see Figure S1 in the Supporting Information).

$$\varepsilon_{620} = \alpha\varepsilon_{M} + (1-\alpha)\varepsilon_{M_2} \quad (2)$$

First, the molar absorptions of the monomer M^{7-} ($\varepsilon_M = 500\,L\,mol^{-1}\,cm^{-1}$) and the dimer M_2^{14-} ($\varepsilon_{M_2} = 1250\,L\,mol^{-1}\,cm^{-1}$) were roughly determined at the limits of the curve presented in Figure 5 and then subsequently optimised by the following theoretical treatments. In particular, the linear Equation (4) should be verified with a slope close to the value of the main constant of the Debye–Hückel law ($A = 0.509\,L^{1/2}\,mol^{-1}$, see below and Figures S1 and S2 in the Supporting Information). The concentrations at the equilibrium of the two species are then calculated from the α parameter. Nevertheless, the determination of the thermodynamic constant $K_d(2)$ for equilibrium (1) needs corrections because the ionic strength μ varies from about 0.03 to 0.3. The activity coefficient γ_i for an ion i is expressed by the extended Debye–Hückel law [Eq. (3)], in which A and B are two defined constants (at 25 °C in water, $A = 0.509\,L^{1/2}\,mol^{-1}$ and $B = 0.347 \times 10^8\,L^{1/2}\,mol^{-1/2}\,cm^{-1}$), z_i is the ionic charge and r_i is a fitting parameter corresponding to the hard-sphere collision distance for a given ion i. Usually, the r_i parameter matches the hydrodynamic radius of the ion.

$$\log_{10}\gamma_i = -\frac{z_i^2 A\sqrt{\mu}}{1 + Br_i\sqrt{\mu}} \quad (3)$$

Equation (4) is then obtained from Equation (3), in which K' is the conditional constant expressed in terms of the concentration of the M_2^{14-} and M^{7-} species and r_M and r_{M_2} are two adjustable parameters associated with the monomeric M and dimeric M_2 species, respectively (see Figure S1 in the Supporting Information).

$$\log_{10}K'(2) = \log_{10}K_d(2) + \frac{98A\sqrt{\mu}}{1 + Br_M\sqrt{\mu}} - \frac{196A\sqrt{\nu}}{1 + Br_{M_2}\sqrt{\nu}} \quad (4)$$

The best linear fit ($R = 0.9974$) was obtained with the current values of the B constant ($0.347 \times 10^8\,L^{1/2}\,mol^{-1/2}\,cm^{-1}$), $r_M = 15 \times 10^{-8}$ cm and $r_{M2} = 17 \times 10^{-8}$ cm, consistent with the dimensions of the involved species, about 25 Å in diameter. The graphical treatment gives $K_d(2) \approx 930\,mol\,L^{-1}$ for the dissociation equilibrium of **2**, expressed by Equation (1). The ε_{620} values calculated from the molar absorptions of the two species and from $K_d(2) = 930\,mol\,L^{-1}$ are in satisfactory agreement with the experimental data (Figure 5), rendering appropriate the supramolecular association model in solution.

Complexation of Ag^+ with 2: Reaction of Ag^+ with **2** provokes a strong increase in absorbance in the visible region (see Figure 4 and Table 1). A spectrophotometric titration of the Ag^+ ion, carried out at 620 nm (Figure S3 in the Supporting Information) clearly indicates that the reaction leads quantitatively to a 2:1 complex (two Ag^+ ions per dimer) and is consistent with the X-ray structure of **2**. The coordination process of Ag^+ was also studied by a potentiometric method by using a silver metal electrode. From the experimental Ag^+/Ag^0 potential (E vs. Ag/AgCl) and the experimental standard potential ($E° = 0.545$ V vs. Ag/AgCl), pAg values were extracted (Figure 6). A pAg jump is observed for two equivalents of Ag^+ ($x = 2$), in agreement with the UV/Vis titration. However, a cooperative or successive process could be invoked for the addition of the two Ag^+ ions to **2**. Cooperative addition (simultaneous complexation of two Ag^+ cations per dimer) leads to Equation (5), in which β corresponds to the equilibrium constant associated with the cooperative process. At semi-equivalence ($x = 1$), the relationship $p\mathrm{Ag} = -{}^1/_2 p\beta$ gives $\beta = 9.45 \times 10^{11}$. pAg is then merely calculated for $0 < x < 2$, but clearly the corresponding calculated curve does not fit the experimental data (Figure 6). Alternatively, pAg can also be calculated on the basis of successive Ag^+ exchange, expressed by Equations (6) and (7).

Table 1. UV/Vis data for anion solutions (3.5×10^{-3} M).

anion	λ [nm]	ε [$L\,mol^{-1}\,cm^{-1}$]
$[M_2]^{12-}$ (**2**)	620	1000
$[Ag_2M_2]^{10-}$ (**3**)	654	2040
	585	4850
$[CuM_2]^{11-}$ (**4**)	705	2770
	585	4630

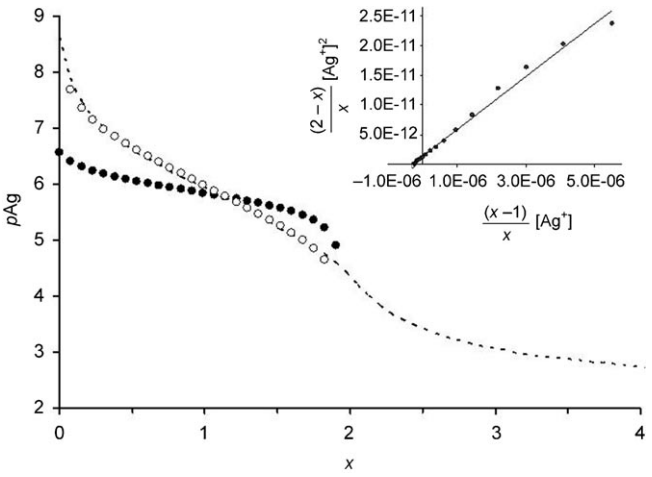

Figure 6. Potentiometric study of the formation of Ag^+ complexes. Dotted line: experimental pAg versus x(x=[Ag^+]/[dimer]). ●: pAg values calculated from a cooperative process. ○: pAg values calculated according to a successive process using the K_1 and K_2 constants. Inset: linear plot of the Equation (8) ($R^2 = 0.9885$) to give $K_1 = 4.1 \times 10^6$ and $K_2 = 2.3 \times 10^5\,L\,mol^{-1}$.

$$p\mathrm{Ag} = \frac{1}{2}p\beta + \frac{1}{2}\log\left[\frac{2-x}{x}\right] \quad (5)$$

$$M_2^{14-} + Ag^+ \rightleftharpoons M_2Ag^{13-} \quad (6)$$

$$M_2Ag^{13-} + Ag^+ \rightleftharpoons M_2Ag_2^{12-} \quad (7)$$

The equilibrium constants K_1 and K_2 associated with Equations (6) and (7) are expected to be large enough to es-

tablish linear Equation (8). As the [Ag^+] activity is calculated from the experimental pAg values, the graphical treatment $\frac{(2-x)}{x}[Ag^+]^2$ versus $\frac{(x-1)}{x}[Ag^+]$ (shown in the inset in Figure 6) results in a straight line, which gives $K_1 = 4.1 \times 10^6$ and $K_2 = 2.3 \times 10^5$ L mol^{-1}. Calculated and experimental pAg values give a satisfactory fit (see Figure 6), rendering the successive coordination model appropriate. Note that such a successive exchange process is only possible with the retention of the supramolecular arrangement in solution, which provides two distinct sites for coordination.

$$\frac{(2-x)}{x}[Ag^+]^2 = \frac{1}{K_2}\frac{(x-1)}{x}[Ag^+] + \frac{1}{K_1 K_2} \quad (8)$$

Stability of the supramolecular anion 3: The behaviour of **3** was studied in solution by UV/Vis spectroscopy. As the concentration increases, the molar absorption at 654 nm increases significantly by about a factor of 2.5 (Figure 7). As postulated for **2**, the dissociation of **3**, as represented in Equation (9), could take place. A similar mathematical treatment to that used for **2** was carried out and leads to $K_d(3) \approx 60$ mol L^{-1}. (see Figure S4 in the Supporting Information). The extrapolated molar absorptions at 654 nm for $M_2Ag_2^{16-}$ and MAg^{8-} are 2140 and 800 L mol^{-1} cm^{-1}, respectively. Such parameters give a satisfactory fit between the experimental and calculated ε_{654} values (see Figure 7). The $K_d(3)$ value is significantly lower than $K_d(2)$ ($K_d(2) \approx 930$ mol L^{-1}), which means that the stability of the supramolecular assembly is significantly reinforced by the presence of two Ag^+ ions that act as coordination linkers between the two monomeric subunits.

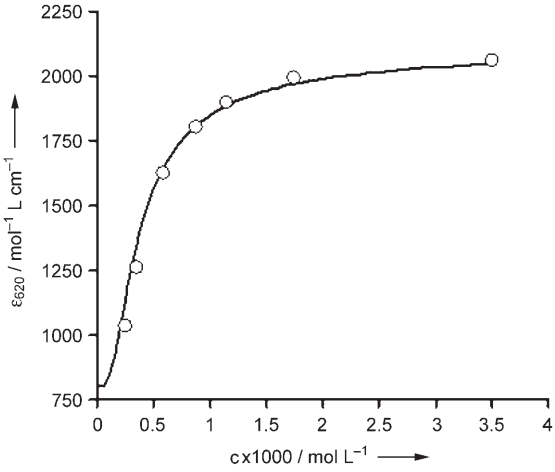

Figure 7. Variation of the molar absorption of **3** at 620 nm with concentration. Experimental (○) and values calculated with $K_d(3) = 60$ (——).

$$M_2Ag_2^{16-} \rightleftharpoons 2MAg^{8-} \quad (9)$$

Complexation of Cu^+ with 2: The addition of Cu^+ ions (as CuI) to **2** produces the expected changes in the visible region already observed with the cuboidal derivatives $\{Mo_3S_4Cu\}^{5+}$.[21] A titration experiment (shown in Figure 8a) carried out with a dilute solution (1.4×10^{-3} mol L^{-1} in **2**) reveals a continuous change in absorbance at 480 nm until a break point at two CuI per dimer. By using a more concentrated solution (3.2×10^{-3} mol L^{-1} in **2**), the absorptions at 697 and 580 nm increase to a maximum for $x = 1$ and then decrease progressively until $x = 2$. The UV/Vis spectrum of the 2:1 complex is fully restored at x = 2 (Figure 8b). It is concluded that two copper-containing complexes are successively formed. At low concentrations and irrespective of the CuI/dimer ratio, the complex with the 2:1 stoichiometry is predominant. Conversely, at higher concentrations, a 1:1 complex is evidenced which corresponds to the stoichiometry of the anion **4**, structurally characterised by X-ray diffraction.

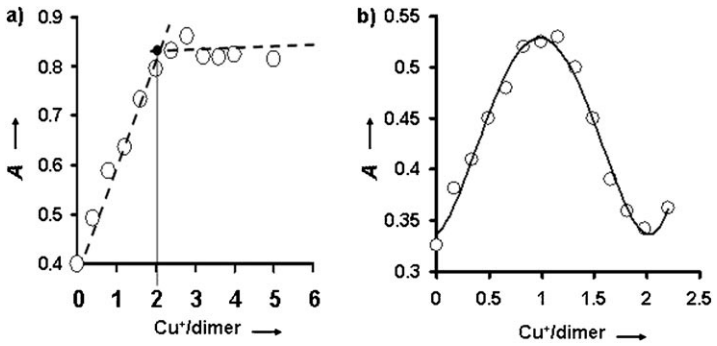

Figure 8. UV/Vis titrations of **2** with CuI. Experiments carried out on a) **2** (1.4 mM) for absorbance measured at 480 nm; b) **2** (3.2 mM) for absorbance measured at 580 nm.

A study of the concentration effects provides complementary evidence concerning the copper-containing species. The UV/Vis spectra of the anion **4** in the high concentration range (7×10^{-3} mol L^{-1}) exhibit characteristics of the 1:1 complex previously evidenced, but dilution of **4** results in a drastic decrease of the two absorptions at 584 and 705 nm (Figures 9 and 10a). Still, a dissociation equilibrium is in-

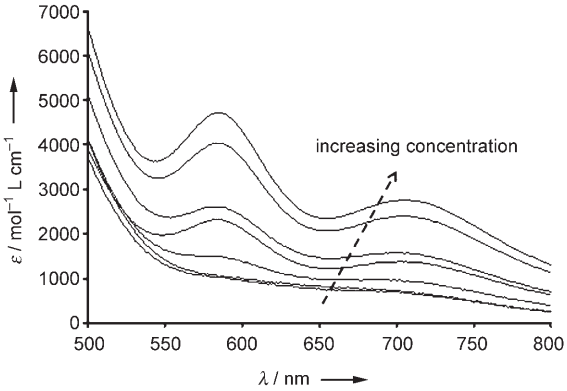

Figure 9. UV/Vis spectra of **4** recorded between 0.35 and 3.5 mM of **4**.

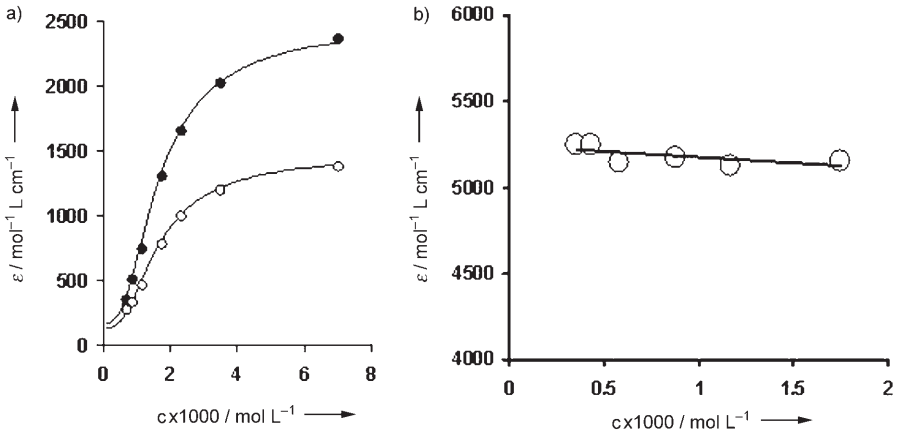

Figure 10. Variation of the molar absorption with the concentration of a) **4** (1:1 complex) measured at 548 (black circles) and 705 nm (white circles) and b) the 2:1 complex measured at 472 nm.

voked in accord with Equation (10), associated with the equilibrium constant $K_d(4)$. In the iodide-free medium, the coordination sphere of the tetrahedral Cu^+ ion within the monomeric moiety is probably completed by an aquo ligand, similar to the aqua ion $[Mo_3S_4Cu(H_2O)_{10}]^{5+}$ described previously.[21] As already carried out for **2** and **3**, treatment of the UV/Vis data led to $K_d(4) \approx 16\ mol\,L^{-1}$, which gives good agreement between the calculated and experimental molar absorbances (see Figure 10a and Figure S4 in Supporting Information). At the same time, the UV/Vis spectrum of the 2:1 complex is not significantly concentration-dependent (Figure 10b). This is consistent with the presence of monomeric species, unable to dimerise because of Cu–Cu repulsions or because of unfavourable steric interactions owing to a possible Cu–I bond within the $\{Mo_3S_4CuI\}^{4+}$ cores.[22] Successive additions of sodium iodide to a solution of **4** ($3\times10^{-2}\ mol\,L^{-1}$ result in a gradual decrease of the absorptions at 697 and 580 nm (not shown), previously attributed to dimeric association. Hence, it can be concluded that the presence of iodide leads to the formation of a Cu–I bond in **4** and subsequently provokes the dissociation of the supramolecular dimer into monomeric components [see Eq. (11)].

$$M_2Cu^{13-} \rightleftharpoons MCu^{6-} + M^{7-} \quad (10)$$

$$M_2Cu^{13-} + I^- \rightleftharpoons M^{7-} + \{MCu{-}I\}^{7-} \quad (11)$$

^{183}W NMR spectroscopy: The ^{183}W NMR spectra and data for **1** to **4** are shown in Figure 11 and Table 2, respectively. The resonances fall in the range of −80 to −200 ppm, which is usually observed for W^{VI} atoms in an octahedral oxo environment.[23] Although some accidental overlaps could occur, the ^{183}W NMR spectra of **1** to **4** are interpreted to be ten lines divided into two sets of five resonances with relative

Table 2. ^{183}W NMR spectral data of sodium salts of **1** to **4** and $[MCuI]^{6-}$.

	δ [ppm] (intensity ratio)
Na-1	−88.2(2), −93.1(2), −106.7(2), −114.5(2×2), −116.6(2), −119.6(2), −126.4(1), −139.4(2), −182.6(1)
Na-2	−89.2(2), −100.6(2), −106.0(2), −114.0(2), −116.1(2), −124.1(2), −125.0(2), −139.5(2), −141.8(1), −187.3(1)
Na-3	−89.0(2×2), −98.1(2), −106.1(2), −107.4(2), −109.0(2), −118.5(2), −124.5(2), −139.8(1), −152.9(1)
Na-4	−87.5(1), −106.3(2), −107.3(2), −118.5(2), −121.8(2), −125.9(2), −133.9(2), −138.2(1), −141.6(2), −186.4(1)
Na_6[MCuI]	−93.8(2), −106.7(2), −117.7(2), −118.5(2), −120.6(2), −122.6(2), −130(1), −136.0(2), −140.8(2), −184.6(1)

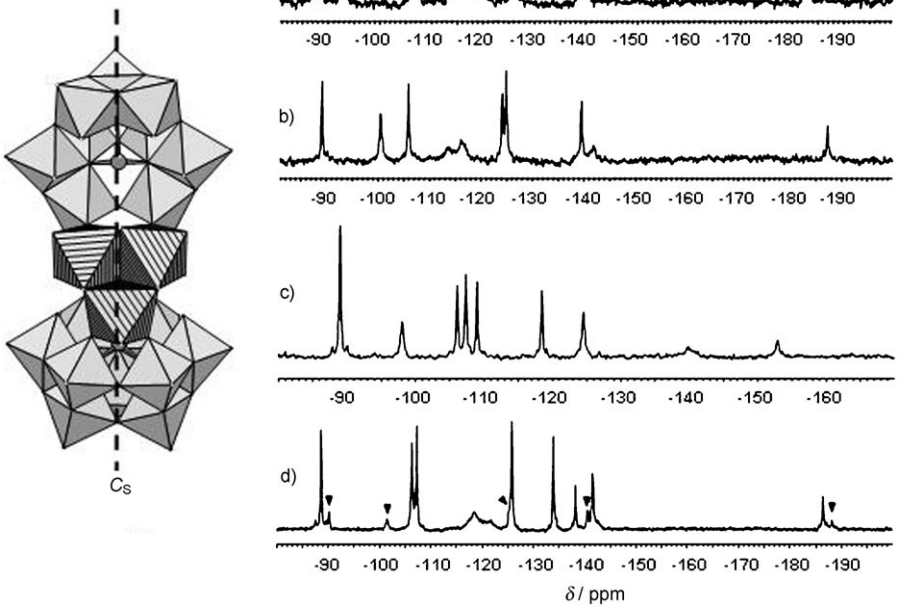

Figure 11. ^{183}W NMR spectra of a) **1**, b) **2**, c) **3** and d) **4** and a basic representation of the monomeric subunit (C_s symmetry). The arrows in the spectrum of **4** identify the resonances attributed to the presence of the anion **2** (≈10%).

intensities of 1:2:2:2:2 (Figure 11). These two sets are attributed to the two $\{AsW_9O_{33}\}$ subunits of C_s symmetry present in each monomeric moiety. Therefore the local C_s symmetry observed in solution for the monomeric moieties is greater than that determined in the solid state (no local symmetry within each constitutive monomer). In addition, ^{183}W NMR spectra were obtained from concentrated solutions (about 0.1–0.3 mol L^{-1} in the dimeric anion), which correspond to conditions in which the supramolecular associations are maintained.

The spectrum of **Na-1** (Figure 11a) exhibits very broad resonances ($\Delta\nu_{1/2}$ = 10–20 Hz); for such large clusters, line widths of only about 5 Hz would be expected.[24] Such line-broadening could be related to the flexible and labile arrangement. The $\{Mo_3S_4\}$ cores act as hinges between two $\{AsW_9O_{33}\}$ units and are able to wriggle within the non-rigid supramolecular complex.

The presence of the two outer $\{AsOH\}^{2+}$ groups in **2** results in significant changes in the 10-line ^{183}W NMR spectrum of **1** (Figure 11b), which is consistent with the retention of these groups in solution.

Although two lines arising from two distinct pairs of tungsten atoms overlap at $\delta = -89.0$ ppm in the ^{183}W NMR spectrum of **Na-3** (Figure 11c), it should be interpreted as a 10-line spectrum. However, the C_{2h} symmetry in solution is understandable only on the basis of the fast hopping of the Ag^+ ions between two equivalent sites. Such a result was nearly suggested in the solid state in which the oblate shapes of the thermal ellipsoids along a common direction seem to illustrate the delocalisation pathway of the Ag^+ ion.

The 10-line ^{183}W NMR spectrum of **Na-4** (Figure 11d) suggests that the single Cu^+ ion is not fixed at either of the two equivalent positions found by crystallography but is delocalised between them. However, compound **4** is not pure in the NMR sample as the presence of the anion **3** (about 10%) is readily identified by its characteristic chemical shifts.

Such fast hopping of the Ag^+ and Cu^+ ions embedded in the POM framework is striking behaviour and probably originates from the unique supramolecular character of the labile and flexible inorganic backbone.

A mixture of **2** and two equivalents of CuI gives a spectrum distinct from that of **4** (Figure S6 in the Supporting Information) and should correspond to the $[MCuI]^{6-}$ monomer previously characterised by UV/Vis spectroscopy. The ^{183}W NMR spectrum obtained from a mixture of **2** and one equivalent of CuI is consistent with the presence of three different compounds, as clearly evidenced in the high and low frequency regions (−85/−95 ppm and −180/−190 ppm) (Figure S5 in the Supporting Information). On the basis of their chemical shifts, these species are readily identified as copper-free anion **2** (denoted M_2^{14-}), 1:1 complex **4** (denoted M_2Cu^{13-}) and monomer $[MCuI]^{6-}$. The copper-containing system can then be fully described by a global equilibrium involving iodide ions and the POM species M_2^{14-}, M_2Cu^{13-} and $MCuI^{6-}$.

Conclusion

This study shows that $[AsW_9O_{33}]^{9-}$ and $[Mo_3S_4(OH_2)_9]^{4+}$ react to give a flexible sandwich monomer that forms a dimer through weak intermolecular interactions. Such a supramolecular arrangement produces three types of coordination sites that are able to complex arsenite, silver and copper selectively. The $\{AsOH\}^{2+}$ groups are located at the periphery of the anion, bridging oxygen atoms of the POM subunits. The coordination spheres of Ag^+ require both constitutive moieties, whereas the Cu^+ ions are located in a central pocket that involves a close contact between two $\{Mo_3S_4\}$ cores. Such multi-unit compounds exhibit striking features as a result of the cooperative properties of the two constitutive components, that is, $\{Mo_3S_4\}$ and $\{AsW_9O_{33}\}$, which are crucial for the supramolecular properties and for the coordination of electron-rich metallic cations. Finally, such molecular systems contain complementary functional components such as 1) the POM subunit known for its electron-storage ability and 2) the electroactive $\{Mo_3S_4\}$ core, the link for the stereoselective inclusion of electron-rich metallic cations. Thus, such multifunctional molecular materials are attractive for future investigations in the field of electrocatalysis.

Experimental Section

Synthesis: All reagents were used as purchased without further purification. The starting solution of $[Mo_3S_4(H_2O)_9]^{4+}$ and the POM precursor, $Na_9[AsW_9O_{33}]\cdot 12H_2O$, were prepared according to published procedures.[25] The preparation of the silver-containing anion (**3**) requires chloride-free pure water obtained from a Milli-RO_4 unit followed by Millipore Q purification.

Elemental analyses were performed by the Service Central d'Analyses du CNRS. Water content corresponding to weight loss up to about 250 °C was determined by thermal gravimetric analysis (TGA) by using a TGA-7 Perkin–Elmer apparatus. IR spectra were recorded by using an FTIR Magna 550 Nicolet spectrometer as pressed KBr pellets.

$K_{12}[\{(H_4AsW_9O_{33})_2(Mo_3S_4\{H_2O\}_5)\}_2]\cdot 46H_2O$ (K-1): $Na_9[AsW_9O_{33}]\cdot 12H_2O$ (5.2 g, 1.94 mmol) was added to an aqueous solution of $[Mo_3S_4(H_2O)_9]^{4+}$ (0.039 M; 25 mL) under vigorous stirring and moderate heating (50 °C). Initially, a green precipitate appeared, which gradually disappeared to yield a clear greenish-brown solution; the solution was simultaneously maintained at pH 2 by the addition of 1 M HCl. Stirring was continued for 30 min and then KCl (5.2 g, 69.7 mmol) was added. The solution was left to stand in an ice bath to complete the precipitation. After 1 h, a dark-green crystalline product was isolated (5.3 g, approx. 92% (based on W)). Elemental analysis calcd (%) for $W_{36}Mo_6As_4K_{12}S_8O_{188}H_{120}$ **(K-1):** W 57.45, Mo 5.00, As 2.60, K 4.07, S 2.22; found: W 56.85, Mo 4.94, As 2.52, K 4.12, S 2.32.

$K_3(NH_4)_9[\{(H_4AsW_9O_{33})_2(Mo_3S_4\{H_2O\}_5)\}_2]\cdot 48H_2O$ (KNH_4-1): The potassium salt **K-1** was recrystallised from a 0.15 M aqueous solution of NH_4Cl to give mixed potassium–ammonium single crystals suitable for X-ray diffraction. IR: $\tilde{\nu}$ = 955 (m), 876 (m), 793 (m), 709 (m), 484 cm^{-1} (s); elemental analysis calcd (%) for $W_{36}Mo_6As_4K_3S_8O_{190}N_9H_{168}$ **(KNH_4-1):** W 59.36, Mo 5.16, As 2.69, K 1.05, S 2.29, N 1.13; found: W 58.91, Mo 4.95, As 2.72, K 1.15, S 2.31, N 1.24.

$K_{14}[\{(H_2As_2W_9O_{33})(H_4AsW_9O_{33})_2(Mo_3S_4\{H_2O\}_5)\}_2]\cdot 51H_2O$ (K-2): A procedure similar to that described for the preparation of **1** was followed, but $NaAsO_2$ (0.13 g, 1 mmol) was added to the clear solution at pH 2. After stirring for 30 min, potassium salt **K-2** was precipitated with KCl

(5.2 g, 69.7 mmol, approx. 90% (based on W)). IR: $\tilde{\nu}$ = 950 (m), 876 (m), 790 (m), 705 (m), 455 cm^{-1} (s); elemental analysis calcd (%) for $W_{36}Mo_6As_6K_{14}S_8O_{194}H_{134}$ (**K-2**): W 56.99, Mo 4.96, As 3.87, K 4.04, S 2.20; found: W 55.56, Mo 4.88, As 3.76, K 4.21, S 2.29.

$K_8(NH_4)_6[(H_2As_2W_9O_{34})(H_4AsW_9O_{33})\{Mo_3S_4(H_2O)_5\}]_2\cdot 48H_2O$ (KNH_4-2): Single crystals of **2** suitable for X-ray diffraction were obtained by recrystallisation of **K-2** in a 0.15 mol L^{-1} aqueous solution of NH_4Cl. IR: $\tilde{\nu}$ = 955 (m), 876 (m), 793 (m), 709 (m), 484 cm^{-1} (s); elemental analysis calcd (%) for $W_{36}Mo_6As_6K_8S_8N_6O_{192}H_{154}$ (**KNH_4-2**): W 57.62, Mo 5.01, As 3.91, K 2.72; found: W 56.85, Mo 4.82, As 3.85, K 2.86.

$K_{16}[Ag(H_2As_2W_9O_{34})(H_2AsW_9O_{33})\{Mo_3S_4(H_2O)_5\}]_2\cdot 48H_2O$ (K-3): Compound **K-2** (5.7 g, 0.495 mmol) was dissolved in a 0.1 mol L^{-1} aqueous solution of KNO_3 (100 mL). Then a 1 mol L^{-1} aqueous solution of $AgNO_3$ (1.05 mL) was added. The solution instantaneously changed from green to deep brown. The solution was filtered and allowed to stand to crystallise for 3 days. Well-shaped brown crystals were obtained (3.7 g, approx. 60% (based on W)). IR: $\tilde{\nu}$ = 960 (m), 876 (m), 793 (m), 710 (m), 486 cm^{-1} (s); elemental analysis calcd (%) for $W_{36}Ag_2Mo_6As_6K_{16}S_8O_{192}H_{124}$ (**K-3):** W 55.65, Ag 1.76, Mo 4.90, As 3.78, K 5.26, S 2.15; found: W 54.48, Ag 1.84, Mo 4.84, As 3.82, K 5.5, S 2.22.

$K_{13}[Cu\{(H_2As_2W_9O_{33})(H_4AsW_9O_{33})(Mo_3S_4[H_2O]_5)\}_2]\cdot 43H_2O$ (K-4): Compound **K-2** (5.7 g, 0.495 mmol) was dissolved in a 0.4 mL L^{-1} aqueous solution of KCl (100 mL). Under stirring, solid CuI (200 mg, 1.05 mmol) was added, which turned the colour of the solution to brown. The solution was heated at 50 °C for 30 min, then filtered and allowed to stand for crystallisation at room temperature for 3 d. Well-shaped brown crystals were obtained (1.7 g, 30% (based on W)). IR: $\tilde{\nu}$ = 957 (m), 875 (m), 790 (m), 711 (m), 483 cm^{-1} (s); elemental analysis calcd (%) for $W_{36}Mo_6As_6CuK_{13}S_8O_{187}H_{118}$ (**K-4):** W 57.28, Mo 4.98, As 3.89, Cu 0.55, K 4.40, S 2.21; found: W 56.62, Mo 4.76, As 3.81, Cu 0.53, K 4.53, S 2.11.

^{183}W NMR spectroscopy: The NMR spectra of concentrated solutions (1–2 g mL^{-1}) of the polyanions (Na^+ salt) were recorded at 20 °C by using a Bruker AC-300 spectrometer operating at 12.5 MHz in 10 mm (o.d.) tubes. Chemical shifts are referenced to an external 2 M solution of Na_2WO_4 in alkaline D_2O and to α-$[SiW_{12}O_{40}]^{4-}$ as a secondary standard (δ = −103.8 ppm). The saturated aqueous solutions of the sodium salts of **1** to **4** were obtained by cationic exchange of the corresponding K^+ salts through a Dowex 50W-X2 resin in Na^+ form. The eluates were evaporated to dryness and the resulting solids dissolved in a mixture of H_2O/D_2O (v/v) to obtain a concentration of about 0.1 to 0.3 mol L^{-1}. The ^{183}W NMR samples of *x*CuI–**3** (*x* = 1 or 2) were obtained from 100 mL solutions of **Na-2** (2 g, 0.177 mmol; obtained from **K-2** by cationic exchange) that contained the corresponding amount of CuI solid. The NMR samples were obtained from the resulting solutions treated by the experimental procedure described above.

UV/Vis spectrophotometry: UV/Vis spectra were recorded at room temperature by using a Perkin–Elmer Lambda 19 spectrophotometer in the spectral range of 800 to 400 nm with a step size of 0.5 nm and a scan speed of 460 nm min^{-1}. The UV/Vis titrations of **3** against Ag^+ and Cu^+ were carried out by using (1–3) × 10^{-3} mol L^{-1} solutions of **3** that contained increasing amounts of $AgNO_3$ (1 mol L^{-1}) and CuI (0.1 mol L^{-1} in acetonitrile), respectively, and by using calibrated quartz crystal cells.

Potentiometric titrations: Potentiometric titrations of the silver ions were carried out by using a Tacussel Minisis 8000 potentiometer equipped with a silver electrode as the working electrode and an Ag/AgCl reference electrode. The redox potentials were measured in a solution of **K-2** (1.5 × 10^{-3} mol L^{-1}) for successive additions of a silver nitrate solution (0.1 mol L^{-1}). The ionic strength was imposed by the addition of $NaNO_3$ (0.5 mol L^{-1}).

X-ray crystallography: Intensity data collections for **KNH_4-1**, **KNH_4-2**, **K-3** and **K-4** were carried out at room temperature by using a Bruker X8 APEX2 CCD instrument and $Mo_{K\alpha}$ radiation (λ = 0.71073 Å). All crystals were mounted in sealed Lindeman tubes to prevent any loss of crystallisation water. An empirical absorption correction based on the method of Blessing[26] was applied by using the SADABS program.[27] The structures were solved by direct methods and refined by the full-matrix least-squares method by using the SHELX-TL package.[28] Relevant crystallographic data for compounds **KNH_4-1**, **KNH_4-2**, **K-3** and **K-4** are reported in Table 3. Heavier atoms (tungsten and molybdenum) for each structure were initially located by direct methods. The remaining non-hydrogen atoms were located from Fourier differences and were refined with anisotropic thermal parameters. The disordered atoms, alkali cations or oxygen atoms of crystallised water were isotropically refined. For **KNH_4-1** and **KNH_4-2**, the ammonium cations were not located and are probably disordered with the water molecules.

Further details on the crystal structure determinations can be obtained from the Fachinformationszentrum Karlsruhe, 76344 Eggenstein-Leopoldshafen, Germany (Fax: (+49) 7247-808666; e-mail: crystaldata@fiz-karlsruhe.de) on quoting the depository numbers CSD-418395 (**KNH_4-1**), CSD-418393 (**KNH_4-2**), CSD-418396 (**K-3**) and CSD-418394 (**K-4**).

Table 3. Selected crystal structure data.

	KNH_4-1	**KNH_4-2**	**K-3**	**K-4**
formula	$W_{36}Mo_6As_4K_3S_8O_{190}N_9H_{168}$	$W_{36}Mo_6As_6K_8S_8N_6O_{192}H_{154}$	$W_{36}Ag_2Mo_6As_6K_{16}S_8O_{192}H_{124}$	$W_{36}Mo_6As_6CuK_{13}S_8O_{187}H_{118}$
M [g mol^{-1}]	11317.9	11639.3	12053.47	11688.0
T [K]	293(2)	293(2)	293(2)	293(3)
crystal size [mm]	0.16 × 0.12 × 0.04	0.15 × 0.10 × 0.06	0.15 × 0.12 × 0.06	0.24 × 0.10 × 0.03
crystal system	triclinic	triclinic	triclinic	triclinic
space group	$P\bar{1}$	$P\bar{1}$	$P\bar{1}$	$P\bar{1}$
a [Å]	13.0244(3)	13.1428(4)	13.1872(6)	13.1001(2)
b [Å]	19.8653(6)	20.9053(6)	20.9825(10)	21.0531(4)
c [Å]	21.1113(6)	21.8562(8)	21.9243(12)	21.9271(4)
α [°]	85.1770(10)	109.624(2)	110.113(2)	110.0210(10)
β [°]	80.0600(10)	95.897(2)	96.327(2)	96.5240(10)
γ [°]	80.1960(10)	101.338(2)	100.665(2)	100.6700(10)
V [Å^3]	5293.2(3)	5452.5(3)	5497.9(5)	5480.17(17)
Z	1	1	1	1
ρ_{calcd} [g cm^{-3}]	3.552	3.546	3.641	3.543
$\mu(Mo_{K\alpha})$ [cm^{-1}]	20.674	20.467	20.507	20.492
θ range [°]	0.98–30.47	1.01–30.00	1.01–30.14	1.01–30.10
data collected/unique	101343/31893	284791/31824	151885/32203	116149/32083
unique data [$I > 2\sigma(I)$]	20808	26034	22791	22088
no. parameters	1210	1258	1180	1189
$R(F)$[a]	0.0470	0.0419	0.0617	0.0442
$R_w(F^2)$[b]	0.1276	0.1205	0.1556	0.1213
GOF	1.062	1.096	1.135	1.115

Acknowledgements

This work was supported by the Centre National de la Recherche Scientifique (CNRS), the Ministère de l'Education Nationale de l'Enseignement Supérieur et de la Recherche (MENESR), the Russian Foundation for Basic Research (Grant 06-03-32831), by a Presidential Grant (MD-7072.2006.03) and by the SupraChem France-Russia Network.

[1] D. L. Long, E. Burkholder, L. Cronin, *Chem. Soc. Rev.* **2007**, *36*, 105–121.
[2] For a selection of reviews, see: a) *Polyoxometalate Chemistry for NanoComposite Design* (Eds.: T. Yamase, M. T. Pope), Kluwer Academic/Plenum, New York, **2002**, pp. 1–127; b) *Chem. Rev.* **1998**, *98*, 1–387 (multiauthor special issue (Ed.: C. L. Hill)); c) M. Misono, *Chem. Commun.* **2001**, 1141–1152.
[3] R. Contant, G. Hervé, *Rev. Inorg. Chem.* **2002**, *22*, 63–111.
[4] U. Kortz, F. Hussain, M. Reicke, *Angew. Chem.* **2005**, *117*, 3839–3843; *Angew. Chem. Int. Ed.* **2005**, *44*, 3773–3777.
[5] a) E. Cadot, V. Béreau, S. Halut, F. Sécheresse, *Inorg. Chem.* **1996**, *35*, 3099–3106; b) V. Béreau, E. Cadot, H. Bögge, A. Müller, F. Sécheresse, *Inorg. Chem.* **1999**, *38*, 5803–5808; c) J. Marrot, M. A. Pilette, F. Sécheresse, E. Cadot, *Inorg. Chem.* **2003**, *42*, 3609–3615.
[6] D. Coucouvanis, A. Toupadakis, A. Hadjikyriacou, *Inorg. Chem.* **1988**, *27*, 3272–3273.
[7] a) F. A. Cotton, Z. Dori, R. Llusar, W. Schwotzer, *J. Am. Chem. Soc.* **1985**, *107*, 6734–6735; b) P. Kathirgamanathan, M. Martinez, A. G. Sykes, *J. Chem. Soc., Chem. Commun.* **1985**, 953–954.
[8] a) T. Shibahara, H. Kuroya, K. Matsumoto, S. Ooi, *Inorg. Chim. Acta* **1986**, *116*, L25–L27; b) M. Martinez, B.-L Ooi, A. G. Sykes, *J. Am. Chem. Soc.* **1987**, *109*, 4615–4619; c) C. Sharp, A. G. Sykes, *J. Chem. Soc., Dalton Trans.* **1988**, 2579–2583.
[9] T. Shibahara, *Coord. Chem. Rev.* **1993**, *123*, 73–147.
[10] E. Cadot, M. A. Pilette, J. Marrot, F. Sécheresse, *Angew. Chem.* **2003**, *115*, 2223–2226; *Angew. Chem. Int. Ed.* **2003**, *42*, 2173–2176.
[11] A. Müller, V. P. Fedin, C. Kuhlmann, H. Bögge, B. Hauptfleisch, H. D. Fenske, B. Baum, *Chem. Commun.* **1999**, 1189–1190.
[12] N. V. Izarova, M. N. Sokolov, E. Cadot, J. Marrot, F. Sécheresse, V. P. Fedin, *Russ. Chem. Bull.* **2004**, *53*, 1503–1506.
[13] a) T. Yamauchi, H. Takagi, T. Shibahara, H. Akashi, Inorg. Chem. **2006**, *45*, 5429–5437; b) M. N. Sokolov, V. P. Fedin, A. G. Sykes, *Compr. Coord. Chem.* **2003**, *3*, 761–823; c) R. Hernandez-Molina, M. N. Sokolov, A. G. Sykes, *Acc. Chem. Res.* **2001**, *34*, 223–230; d) R. Llusar, S. Uriel, *Eur. J. Inorg. Chem.* **2003**, 1271–1290.
[14] M. Nasreldin, Y.-J. Li, F. E. Mabbs, A. G. Sykes, *Inorg. Chem.* **1994**, *33*, 4283–4289.
[15] T. Murata, H. Gao, Y. Mizobe, F. Nakano, S. Motomura, T. Tanase, S. Yano, M. Hidai, *J. Am. Chem. Soc.* **1992**, *114*, 8287–8288.
[16] R. Hernandez-Molina, L. Kalinina, M. N. Sokolov, M. Clausen, J. Gonzalez-Platas, C. Vicent, R. Llusar, *Dalton Trans.* **2007**, 550–557.
[17] V. P. Fedin, M. N. Sokolov, D. N. Dybtsev, O. A. Gerasko, A. V. Virovets, D. Fenske, *Inorg. Chim. Acta* **2002**, *331*, 31–38.
[18] M. Leyrie, A. Tézé, G. Hervé, *Inorg. Chem.* **1985**, *24*, 1275–1277.
[19] T. Shibahara, H. Akashi, H. Kuroya, *J. Am. Chem. Soc.* **1988**, *110*, 3313–3314.
[20] D. T. Richens, P.-A. Pittet, A. E. Merbach, M. Humanes, G. J. Lamprecht, B.-L. Ooi, A. G. Sykes, *J. Chem. Soc., Dalton Trans.* **1993**, 2305–2311.
[21] M. Nasreldin, Y.-J. Li, F. E. Mabbs, A. G. Sykes, *Inorg. Chem.* **1994**, *33*, 4283–4289.
[22] W. Xinato, L. Shaofeng, Z. Lianyong, W. Qjangin, L. Jiaxi, *Inorg. Chim. Acta* **1987**, *133*, 39–42.
[23] Y.-G. Chen, J. Gong, L.-Y. Qu, *Coord. Chem. Rev.* **2004**, *248*, 245–260.
[24] G. M. Maksimov, R. I. Maksimovskaya, G. S. Litvak, *Russ. J. Inorg. Chem.* **2005**, *50*, 1062–1065.
[25] C. Tourné, A. Revel, G. Tourné, M. Vendrell, *C. R. Seances Acad. Sci. Ser C* **1973**, *277*, 643–645.
[26] R. Blessing, *Acta Crystallogr., Sect. A* **1995**, *51*, 33.
[27] SADABS, program for scaling and correction of area detector data, G. M. Sheldrick, University of Göttingen (Germany), **1997**.
[28] a) G. M. Sheldrick, *Acta Crystallogr. Sect. A* **1990**, *46*, 467; b) SHELX-TL, version 5.03, Software Package for Crystal Structure Determination, G. M. Sheldrick, Siemens Analytical X-ray Instrument Division, Madison, WI, **1994**.

Received: July 25, 2007
Published online: February 18, 2008

